An Angle-Based Control Law for Target Location Stabilization in 3D Space

Liangming Chen, Ruizhi Ruan, Jianqing Li, Weijie Yuan, and Zhiyun Lin, *Fellow, IEEE*

***Abstract*— Many aerial tasks require an aircraft to move to a target location autonomously. However, existing linear control laws usually require absolute/relative position measurements with respect to the target location, and nonlinear distance-only control laws merely guarantee local convergence to the target location. Motivated by this challenge, we propose a 3-D angle-based control law such that an aircraft can autonomously move to the target location described by three angle constraints with respect to three ground stations. The proposed control law only needs bearing measurements and communication between the aircraft and the ground stations. By decoupling the dynamics of the angle errors, the proposed control law for single-integrator dynamics guarantees global convergence to the target location. Three angles are controlled to converge, which are independent of the orientation of the aircraft's coordinate frame. This control law is more accessible and reliable than those based on relative position. Simulations are conducted to validate the effectiveness of the proposed control law.**

***Index Terms*— Autonomous navigation, nonlinear control, bearing measurements, angle-based control and stability analysis.**

I. Introduction

Autonomous control of Unmanned Aerial Vehicles (UAVs) plays a pivotal role in various practical applications, including aerial photography, logistical delivery, search and rescue operations, and intelligent agriculture [1]–[3]. The aim of autonomous control is to guide vehicles from an arbitrary initial position to a specified target position. Autonomous control entails the integration of advanced control algorithms, sensor units, and decision-making processes to enable the vehicle to produce efficient control actions such that it can reach the desired target position [4]. There are generally two types of control techniques, namely direct control through obtained sensor measurements (such as distance) [5] and indirect control through localization (such as visual-inertial odometry) [6], whereas this work only focuses on direct control.

This work is supported by Shenzhen Key Laboratory of Control Theory and Intelligent Systems under Grant ZDSYS20220330161800001.

Liangming Chen, Weijie Yuan and Zhiyun Lin are with Shenzhen Key Laboratory of Control Theory and Intelligent Systems, School of Automation and Intelligent Manufacturing, Southern University of Science and Technology, Shenzhen, China (email: chenlm6@sustech.edu.cn, yuanwj@sustech.edu.cn, linzy@sustech.edu.cn).

Ruizhi Ruan is with National Graduate College for Engineers, Southern University of Science and Technology, Shenzhen, China (email: ruanrz@mail.sustech.edu.cn).

Jianqing Li is with College of Communication Engineering, Hangzhou Dianzi University, Hangzhou, China (email: jianqing@hdu.edu.cn).

Both linear and nonlinear approaches are proposed for achieving the control task, where the linear ones include position-based and relative position-based appraoches and the nonlinear ones mainly include bearing-based, distance-based, and angle-based approaches [7]. Position-based control relies on measurements of the vehicle's absolute position using sensors such as GPS receiver or other global positioning systems. However, GPS signals become weak in deep sea, indoor space, and forest [8]. Relative position-based control only requires the vehicle to measure relative positions with respect to (w.r.t) at least one ground station or landmark, in which the target position can be described by the relative position w.r.t the ground station. One restriction of relative position-based control is that the vehicle's coordinate frame used for relative position measurements should have the same orientation as the coordinate frame used for describing the target position, which can be hard to be perfectly satisfied [9], [10]. Different from the aforementioned linear control approaches, nonlinear control approaches describe the target position via several nonlinear quantities, such as two bearings, three distances, or three angles w.r.t some ground stations, in which the required measurements become bearings, distances, or local bearings/directions w.r.t the ground stations, respectively. One main advantage of nonlinear control is the reduction on the needed sensor units for the relative measurements between the vehicle and the ground stations. However, the bearing-based control approach suffers from the same issue as the relative position-based control, namely the orientation of the coordinate frames needs to be the same [11]. Although distance-based and angle-based control does not suffer from the issue on coordinate frames, their existing control laws usually only guarantee local convergence to the target position [5], [12], [13]. It is worth mentioning some distance-based control laws indeed achieve global convergence, in which, however, additional measurements for relative localization are needed, such as the vehicle's self-displacements [6], [14].

Motivated by the aforementioned aspects, this note aims to design an angle-based control law which guarantees global convergence and only needs bearing measurements in the vehicle's local coordinate frame. As illustrated in [13, Section IV], the formulated problem is challenging due to the asymmetric and non-diagonal system matrix in the highly nonlinear closed-loop dynamics of the angle errors in 3-D. It was also stated in [15, Section 2.3] that a suitable Lyapunov function had not been found in 2-D. Different from these previous works [11]–[13], [15] where all control components are formed by the multiplication of inter-bearing angle errors with inter-vehicle

bearing vectors, we propose a novel control law in this work where the key control component is formed by the multiplication of inter-plane angle errors with the cross product of inter-vehicle bearing vectors. The key advantage of this design is the decoupling of angle error dynamics, which renders the closed-loop system matrix diagonal and ensures global convergence. The contributions are twofold: the control law guarantees global convergence to the target, and the required angles are independent of the vehicle's frame, making them more reliable and accessible than relative positions. Target navigation is a fundamental task, and specifying it via angle constraints has clear physical meaning: the constraints are frame-independent and require only local bearing measurements, which are easier to obtain than positions. This makes the method suitable for GPS- and inertial-denied environments, such as deep-space navigation.

The rest of this note is organized as follows. Section II introduces the preliminaries. The angle-based control for the single-integrator and quadrotor models is given in Sections III and IV, respectively. Simulations are given in Section V.

II. Preliminaries and Problem Formulation

A. Notations

Consider the system consisting of an aircraft whose position is $p_0 \in \mathbb{R}^3$, and three static ground stations whose positions are $p_1 \in \mathbb{R}^3, p_2 \in \mathbb{R}^3, p_3 \in \mathbb{R}^3$, respectively. We assume that p_1, p_2, p_3 are non-collinear and non-overlapping. We also assume that the aircraft holds an unknown coordinate frame $\sum_0$ for sensor measurements and control execution, and each of the three ground stations also hold an unknown coordinate frame $\sum_1, \sum_2, \sum_3$ for sensor measurements. Let I_3, 1_n, $\otimes$, $\lambda_{\max}$, $\lambda_{\min}$, $\det()$ be the 3-by-3 identity matrix, $n \times 1$ column vector of all ones, the Kronecker product, the maximum eigenvalue, the minimum eigenvalue of a symmetric matrix, and the determinant of a square matrix, respectively. Denote by $R_g^i \in SO(3), i = 0, 1, 2, 3$ the 3D rotation matrix from the global coordinate frame $\sum_g$ to $\sum_i$. Denote by p_i, p_i^j the position of i in $\sum_g, \sum_j$, respectively. Denote by $\mathbb{P}_{ijk}$ the plane formed by p_i,p_j,p_k. The positive direction of $\mathbb{P}_{ijk}$ is formed by $i \to j \to k$ under the right hand screw rule. Conversely, the negative direction of $\mathbb{P}_{ijk}$ is formed by $k \to j \to i$ under the right hand screw rule.

B. Bearing measurements and angle information

Define the direction from p_i to p_j in $\sum_g$ as a unit vector

$$b_{ij} = \frac{p_j - p_i}{\|p_j - p_i\|}, i, j \in \{0, 1, 2, 3\}, i \neq j \tag{1}$$

which is also called as bearing measurements in this note. Then, the local bearing vectors b_{ij} measured in $\sum_i$ is $b_{ij}^i = R_g^i b_{ij}$. From the bearing vectors b_{ij}, b_{ik}, one has the magnitude of the interior angle α_{jik} as

$$\alpha_{jik} = \arccos(b_{ij}^\top b_{ik}) \in (0, \pi) \tag{2}$$

The control variables in this note are angles instead of bearings. Since $b_{ij}^\top b_{ik} = b_{ij}^{i\top} b_{ik}^i$, the magnitude of the interior angle α_{jik} in $\sum_g$ is the same as that in $\sum_i$. Note that bearing is defined as a unit vector from one point to the other point. Direction has the same meaning as 'bearing' in most cases. An angle between two bearing vectors can be determined by (2), which is independent of the coordinate frame $\sum_g$ or $\sum_i$.

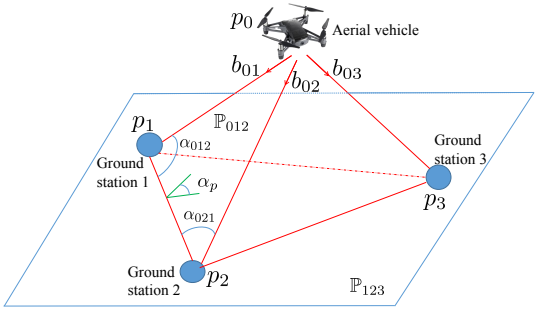

Fig. 1: System consisting of one aerial vehicle and three ground stations

C. Problem formulation

Denote $p_0^* \in \mathbb{R}^3$ as the target position that the aircraft aims to autonomously move to, which is time-invariant. And p_0^* can be any point in 3D space. As shown in Fig. 1, we consider that the aircraft does not have a Global Positioning System (GPS) but only has a bearing measurement sensor, such as vision-based camera or directional antenna arrays, which provide local bearing measurements b_{01}, b_{02}, b_{03} w.r.t the ground stations 1, 2 and 3. Note that two methods can be used to obtain such bearings accurately, including vision-based cameras [16] and directional antenna arrays [17]. In addition, when the aircraft operates under dynamic environments, Lidar or vision sensors with depth information are usually required for obstacle avoidance, which is a research topic that has been widely studied [18]. Due to the absence of localizing the aircraft's absolute position and sensing the distance between the aircraft and the stations, the autonomous control task is challenging to solve.

In [11], a similar control task is formulated, which is solved by controlling the bearings from the aircraft to some fixed beacons. The agent's local coordinate frame, such as the sensed inertial frame can be time-varying due to the existence of sensing noise and uncertainty. If the sensed inertial frame is biased and the aircraft still aims to achieve the unbiased desired bearing vectors $b_{01}^*, b_{02}^*, b_{03}^*$ described in the ideal inertial frame, then the aircraft will not reach the target position p_0^* under the same control law. Different from [11] and inspired by the angle definition between two planes in [19], we describe the target position p_0^* by three angles constraints $\alpha_{012}^*, \alpha_{021}^*, \alpha_p^*$, where α_p^* is the desired angle between the plane $\mathbb{P}_{123}$ and the plane $\mathbb{P}_{012}$. Based on the above description, the objective of this control task is to design $\dot{p}_0(t)$ by using the aforementioned available information such that

$$\begin{aligned} &\lim_{t\to\infty}(\alpha_{012}(t) - \alpha_{012}^*) = 0 \\ &\lim_{t\to\infty}(\alpha_{021}(t) - \alpha_{021}^*) = 0 \\ &\lim_{t\to\infty}(\alpha_p(t) - \alpha_p^*) = 0 \end{aligned} \tag{3}$$

where $\alpha^*_{012} = \arccos(b_{10}^{*\top} b_{12}) \in (0,\pi), \alpha^*_{021} = \arccos(b_{20}^{*\top} b_{21}) \in (0,\pi)$, $b^*_{ij} = \frac{p^*_j - p^*_i}{\|p^*_j - p^*_i\|}, i,j \in \{0,1,2,3\}, i \neq j$, $\alpha^*_p \in (-\pi,\pi)$, and $\alpha^*_p = \begin{cases} \arccos(n_{012}^{*\top} n^*_{123}), & \text{if } b_{10}^{*\top} n^*_{123} > 0 \\ -\arccos(n_{012}^{*\top} n^*_{123}), & \text{otherwise} \end{cases}$, $n^*_{012} = \frac{b^*_{20} \times b^*_{21}}{\|b^*_{20} \times b^*_{21}\|}$ and $n^*_{123} = \frac{b^*_{23} \times b^*_{21}}{\|b^*_{23} \times b^*_{21}\|}$ are the normal vectors of the planes $\mathbb{P}^*_{012}$ and $\mathbb{P}^*_{123}$, respectively. Note that the description of p^*_0 by the three angle constraints should be unique to ensure that the aircraft can move to the target location. Thus, we firstly present the following result.

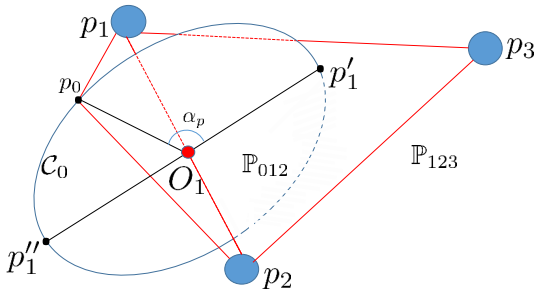

Fig. 2: Unique determination of the target location by three angle constraints

Lemma 1: Given $\alpha^*_{012} \in (0,\pi), \alpha^*_{021} \in (0,\pi)$, $\alpha^*_p \in (-\pi,\pi)$, the target position p^*_0 is uniquely determined.

Proof: First consider the case $\alpha^*_p \in (0,\pi)$. Since p_1, p_2, and p_3 are fixed, as shown in Fig. 2, the angle constraints α^*_{012} and α^*_{021} will allow p_0 to lie in the circle $\mathcal{C}_0$ whose radius is $\|p^*_0 - p_1\| \cos\alpha^*_{012}$ and origin O_1 satisfying $p_2 - p_1 = \frac{\tan\alpha^*_{012} + \tan\alpha^*_{021}}{\tan\alpha^*_{012}}(p_{O_1} - p_1)$. Denote by $p'_1 \in \mathbb{R}^3, p''_1 \in \mathbb{R}^3$ the two intersections of $\mathcal{C}_0$ and $\mathbb{P}_{123}$. Note that when p_0 moves along the circle $\mathcal{C}_0$ from p'_1 to p''_1, the angle α_p changes from 0 to π monotonously. Therefore, given a desired $\alpha^*_p \in (0,\pi)$, its position on the circle $\mathcal{C}_0$ only has two possible solutions, namely one in the upper side of $\mathbb{P}_{123}$ and the other one in the lower side of $\mathbb{P}_{123}$. Since we consider $\mathbb{P}_{123}$ as the ground plane and p^*_0 should be above the ground plane, the position p^*_0 is globally and uniquely determined under the three-angle constraints. When $\alpha^*_p \in (-\pi,0)$, one can also obtain two possible solutions, but only one is correct due to the sign constraint in α^*_p. ■

In the following, we consider the control design for the cases where $p_0(t)$ is governed by single-integrator and quadrotor dynamics, respectively.

III. Angle-based control for single-integrator model

In this part, we assume that the dynamics of the aircraft are governed by a single-integrator

$$\dot{p}_0(t) = u_0(t) \tag{4}$$

To achieve the objective (3), we design the controller $u_0(t)$ as

$$\begin{aligned} u_0(t) =& (\alpha_{012}(t) - \alpha^*_{012}) b_{02}(t) + (\alpha_{021}(t) - \alpha^*_{021}) b_{01}(t) \\ & - (\alpha_p(t) - \alpha^*_p) b_{01}(t) \times b_{02}(t) \end{aligned} \tag{5}$$

where α_p is similar to $\alpha^*_p \in (-\pi,\pi)$, and $\alpha_p = \begin{cases} \arccos(n_{012}^\top n_{123}), & \text{if } b_{10}^\top n_{123} \geq 0 \\ -\arccos(n_{012}^\top n_{123}), & \text{otherwise} \end{cases}$, $n_{012} = \frac{b_{20} \times b_{21}}{\|b_{20} \times b_{21}\|}$ and $n_{123} = \frac{b_{23} \times b_{21}}{\|b_{23} \times b_{21}\|}$. The sign of α_p depends on the direction of p_0 relative to $\mathbb{P}_{123}$. Specifically, when p_0 is in the positive direction of $\mathbb{P}_{123}$, α_p takes a positive value. Conversely, when p_0 is in the negative direction of $\mathbb{P}_{123}$, α_p takes a negative value. Similarly, this property is applicable to α^*_p. The bearing vectors $b_{01}(t)$ and $b_{02}(t)$ can be obtained from bearing measurements. In practice, these required bearings can be measured by vision-based camera or directional antenna arrays. Note that the first component of the controller (5) is a feedback to the angle error $e_1 = \alpha_{012}(t) - \alpha^*_{012}$ because when the aircraft moves towards the bearing vectors b_{02}, $\alpha_{012}(t)$ will decrease. Similarly, the second and third components of (5) are feedback to the angle errors $e_2 = \alpha_{021}(t) - \alpha^*_{021}$ and $e_p = \alpha_p(t) - \alpha^*_p$, respectively. It is worth noting that $b_{01} \times b_{02}$ is perpendicular to b_{01} and b_{02}, which plays an important role in the decoupling and convergence of the three angle errors.

Remark 1: Different from the angle-based law (20) in [13], the controller (5) has different components, specifically different desired angle α^*_p and heading vector $b_{01}(t) \times b_{02}(t)$. These components play an important role in achieving objective (3).

Remark 2: Although the bearing vectors and scalar angles are all described in the global coordinate frame, the control law (5) can be realized in the agent's local coordinate frame. When the agent 0 has a local coordinate frame $\sum_0$ for control execution and measurements, control law (5) can be equivalently written in the local coordinate frame as

$$\begin{aligned} u^0_0(t) &= R^0_g u_0(t) = (\alpha_{012}(t) - \alpha^*_{012}) R^0_g b_{02}(t) + (\alpha_{021}(t) \\ &\quad - \alpha^*_{021}) R^0_g b_{01}(t) - (\alpha_p(t) - \alpha^*_p) R^0_g (b_{01}(t) \times b_{02}(t)) \\ &= (\alpha_{012}(t) - \alpha^*_{012}) b^0_{02}(t) + (\alpha_{021}(t) - \alpha^*_{021}) b^0_{01}(t) \\ &\quad - (\alpha_p(t) - \alpha^*_p)(b^0_{01}(t) \times b^0_{02}(t)) \end{aligned} \tag{6}$$

where $R^0_g \in SO(3)$ is the rotation matrix from the global coordinate frame to the aerial vehicle's local coordinate frame, $R^0_g u_0(t)$ is the controller input in the aerial vehicle's local coordinate frame, and $R^0_g b_{01} = b^0_{01}$ and $R^0_g b_{02} = b^0_{02}$ are the local bearings measured in the vehicle's local coordinate frame. Since R^0_g is invertible and $(\alpha_{012}(t) - \alpha^*_{012}(t))$, $(\alpha_{021}(t) - \alpha^*_{021}(t))$ and $(\alpha_p(t) - \alpha^*_p(t))$ are all scalars (which are invariant under different coordinate frames), the evolution of (6) in $\sum_0$ and the evolution of the control law (5) in $\sum_g$ is equivalent, for which the system convergence is the same when the vehicle has a local coordinate frame.

A. Analysis of angle error dynamics

We first analyze their dynamics to prove the convergence of the angle errors e_1, e_2, e_p. Taking e_1 as an example, one has

$$\begin{aligned} \frac{\mathrm{d}\cos\alpha_{012}}{\mathrm{d}t} &= (-\sin\alpha_{012})\dot{\alpha}_{012} = \dot{b}_{10}^{\mathrm{T}} b_{12} + b_{10}^{\mathrm{T}} \dot{b}_{12} \\ &= [(\frac{P_{b_{10}}}{l_{10}}(\dot{p}_0 - \dot{p}_1)]^{\mathrm{T}} b_{12} + b_{10}^{\mathrm{T}} \frac{P_{b_{12}}}{l_{12}}(\dot{p}_2 - \dot{p}_1), \end{aligned} \tag{7}$$

where $l_{ji} = \|p_j - p_i\|$, $P_{b_{ji}} = I_3 - b_{ji} b_{ji}^{\mathrm{T}}, i,j \in \{0,1,2,3\}, i \neq j$. Using the facts $\dot{p}_i = 0, i = 1,2,3$, one has the dynamics of

e_1

$$\dot{e}_1 = \dot{\alpha}_{012} = -\frac{b_{12}^\top P_{b_{10}} \dot{p}_0}{l_{10} \sin\alpha_{012}} \tag{8}$$

Substituting the control law (5) into (8) yields

$$\dot{e}_1 = -\frac{b_{12}^\top P_{b_{10}} (e_1 b_{02} + e_2 b_{01} - e_p b_{01} \times b_{02})}{l_{10} \sin\alpha_{012}} \tag{9}$$

Note that $P_{b_{10}} b_{01} = b_{01} - b_{01} = 0$, and

$$\begin{aligned} b_{12}^\top P_{b_{10}} (b_{01} \times b_{02}) &= \frac{l_{10} b_{10}^\top + l_{02} b_{02}^\top}{l_{12}} (I_3 - b_{10} b_{10}^\top)(b_{01} \times b_{02}) \\ &= \frac{l_{10} b_{10}^\top + l_{02} b_{02}^\top}{l_{12}} (b_{01} \times b_{02}) = 0 \end{aligned} \tag{10}$$

Substituting (10) into (9) yields

$$\begin{aligned} \dot{e}_1 &= -\frac{b_{12}^\top (I_3 - b_{10} b_{10}^\top) b_{02}}{l_{10} \sin\alpha_{012}} e_1 \\ &= -\frac{\cos(\pi - \alpha_{012} - \alpha_{102}) + \cos\alpha_{012} \cos\alpha_{102}}{l_{10} \sin\alpha_{012}} e_1 \\ &= -\frac{\sin\alpha_{102}}{l_{10}} e_1 \end{aligned} \tag{11}$$

Similarly using (7), one has

$$\dot{e}_2 = -\frac{b_{21}^\top P_{b_{20}} \dot{p}_0}{l_{20} \sin\alpha_{021}} = -\frac{b_{21}^\top P_{b_{20}} (e_1 b_{02} + e_2 b_{01} - e_p b_{01} \times b_{02})}{l_{20} \sin\alpha_{021}} \tag{12}$$

Similarly, one also has $P_{b_{20}} b_{02} = 0$ and $b_{21}^\top P_{b_{20}} (b_{01} \times b_{02}) = 0$. Then, it follows that

$$\begin{aligned} \dot{e}_2 &= -\frac{b_{21}^\top P_{b_{20}} b_{01}}{l_{20} \sin\alpha_{021}} e_2 = -\frac{b_{21}^\top (I_3 - b_{20} b_{20}^\top) b_{01}}{l_{20} \sin\alpha_{021}} e_2 \\ &= -\frac{\cos\alpha_{012} + \cos\alpha_{021} \cos\alpha_{102}}{l_{20} \sin\alpha_{021}} e_2 = -\frac{\sin\alpha_{102}}{l_{20}} e_2 \end{aligned} \tag{13}$$

Now, we analyze the dynamics of e_p. Note that $\cos\alpha_p = \cos(-\alpha_p)$. Then, similarly using (7), one has

$$\begin{aligned} &\frac{\mathrm{d}\cos\alpha_p}{\mathrm{d}t} = (-\sin\alpha_p)\dot{\alpha}_p = \dot{n}_{012}^{\mathrm{T}} n_{123} + n_{012}^{\mathrm{T}} \dot{n}_{123} \\ &= [\frac{P_{n_{012}}}{\|b_{20} \times b_{21}\|} (\dot{b}_{20} \times b_{21} + b_{20} \times \dot{b}_{21})]^{\mathrm{T}} n_{123} \\ &+ n_{012}^{\mathrm{T}} \frac{P_{n_{123}}}{\|b_{23} \times b_{21}\|} (\dot{b}_{23} \times b_{21} + b_{23} \times \dot{b}_{21}) \end{aligned} \tag{14}$$

Since $\dot{p}_i = 0, i = 1, 2, 3$, one has $\dot{b}_{23}^\top \times b_{21} = 0$, $b_{23}^\top \times \dot{b}_{21} = 0$ and $b_{20}^\top \times \dot{b}_{21} = 0$. Then, it follows that

$$\begin{aligned} \dot{e}_p = \dot{\alpha}_p &= -\frac{n_{123}^\top P_{n_{012}} (\frac{P_{b_{20}} \dot{p}_0}{l_{20}} \times b_{21})}{\|b_{20} \times b_{21}\| \sin\alpha_p} \\ &= -\frac{n_{123}^\top P_{n_{012}} ([P_{b_{20}} (e_1 b_{02} + e_2 b_{01} - e_p b_{01} \times b_{02})] \times b_{21})}{l_{20} \|b_{20} \times b_{21}\| \sin\alpha_p} \end{aligned} \tag{15}$$

Note that $P_{b_{20}} b_{02} = 0$ and

$$\begin{aligned} &P_{n_{012}} [(P_{b_{20}} b_{01}) \times b_{21}] \\ =&P_{n_{012}} (b_{01} \times b_{21}) - P_{n_{012}} [(b_{20} b_{20}^\top b_{01}) \times b_{21}] \\ =&- P_{n_{012}} n_{012} \|b_{01} \times b_{21}\| + P_{n_{012}} n_{012} \cos\alpha_{102} \|b_{20} \times b_{21}\| \\ =&0 \end{aligned} \tag{16}$$

where we have used the fact $P_{n_{012}} n_{012} = 0$. On the other hand,

$$\begin{aligned} &n_{123}^\top P_{n_{012}} ([P_{b_{20}} (b_{01} \times b_{02})] \times b_{21}) \\ =&n_{123}^\top P_{n_{012}} ([(I_3 - b_{20} b_{20}^\top)(b_{01} \times b_{02})] \times b_{21}) \\ =&n_{123}^\top (I_3 - n_{012} n_{012}^\top)[(b_{01} \times b_{02}) \times b_{21}] \\ =&n_{123}^\top [(b_{01} \times b_{02}) \times b_{21}] = \frac{\|b_{01} \times b_{02}\|}{\|b_{20} \times b_{21}\|} n_{123}^\top (b_{20} \times b_{21}) \times b_{21} \\ =&- \|b_{01} \times b_{02}\| \|b_{20} \times b_{21}\|^{-1} n_{123}^\top b_{20} \end{aligned} \tag{17}$$

where we have used $n_{123}^\top b_{21} = 0$ and $(b_{20} \times b_{21}) \times b_{21} = b_{21} \cos\alpha_{120} - b_{20}$. Based on geometric relation, one has $n_{123}^\top b_{20} = \cos(\pi/2)\cos\alpha_{120} + \cos(\pi/2 - \alpha_p)\sin\alpha_{120} = \sin\alpha_p \sin\alpha_{120}$ since b_{12} is the common edge of $\mathbb{P}_{123}$ and $\mathbb{P}_{012}$ and $P_{b_{12}} b_{20}$ represents the projection of b_{20} into the orthogonal plane of b_{12} (which is also the plane formed by n_{012} and n_{123}). Using (14)-(17), one has

$$\dot{e}_p = -\frac{\|b_{01} \times b_{02}\|}{l_{20} \|b_{20} \times b_{21}\|^2} e_p = -\frac{\sin\alpha_{102}}{l_{20} \sin\alpha_{021}} e_p \tag{18}$$

Now, writing (11), (13) and (18) into a compact form yields

$$\dot{X} = \begin{bmatrix} \dot{e}_1 \\ \dot{e}_2 \\ \dot{e}_p \end{bmatrix} = -\begin{bmatrix} \frac{\sin\alpha_{102}}{l_{10}} & 0 & 0 \\ 0 & \frac{\sin\alpha_{102}}{l_{20}} & 0 \\ 0 & 0 & \frac{\sin\alpha_{102}}{l_{20} \sin\alpha_{021}} \end{bmatrix} \begin{bmatrix} e_1 \\ e_2 \\ e_p \end{bmatrix} \tag{19}$$

where $X = [e_1, e_2, e_p]^\top$. Note that the overall dynamics system matrix is a diagonal matrix of the overall dynamics (19). However, to analyze its stability, we first need to guarantee the dynamics (19) is well-defined, i.e., $l_{10}(t) \neq 0, l_{20}(t) \neq 0$, $\sin\alpha_{021}(t) \neq 0$for $\forall t > 0$. Therefore, we must first prove that no colliding and no collinear scenarios will occur among $p_0(t)$ and p_1, p_2 under the controller (5).

Remark 3: It is worth mentioning that the constrained angle α_p^* in this paper is different from those in [13]. It can be seen that the diagonal matrix in (19) is more concise than the corresponding one (22) in [13] because of the usage of the constrained angle α_p and the designed control law (5).

B. Analysis of inter-agent collinear scenarios for model (4) under controller (5)

First, we give the following lemma.

Lemma 2: If $p_0(0)$ is bounded away from the line $\overleftrightarrow{p_1 p_2}$, then under the control law (5), $l_{10}(t), l_{20}(t)$ and $\sin\alpha_{021}(t)$ will be bounded away from zero for $\forall t > 0$.

Proof: We first prove that $p_0(t)$ will not collide with $p_1(t)$ and $p_2(t)$ for $\forall t > 0$. Note that the dynamics of e_p in (19) is independent of the dynamics of e_1 and e_2. Suppose on the contrary that there exists a time instant $t = T_0$ such that $p_0(T_0)$ firstly collides with p_1 and no collision occur between p_0 and p_1, p_2 during $[0, T_0)$. Then, the angle dynamics (19) is well-defined for $t \in [0, T_0)$. Clearly, one has $\alpha_{021}(T_0^-) \to 0^+$. However, α_{021}^* is bounded away from 0, and the dynamics of e_2 in (13) implies that e_2 decrease monotonously. This gives a contradiction since e_2 increases from $t = T_0^-$ to T_0. A similar conclusion can be obtained for the collision between p_0 and p_2. Thus, $p_0(t)$ will not collide with p_1 and p_2.

Then, we prove that $p_0(t)$ and p_1, p_2 will not be collinear. Suppose on the contrary that $p_0(t)$ reaches the line $\overleftrightarrow{p_1p_2}$ (corresponding to $\sin\alpha_{021}(t)=0$).

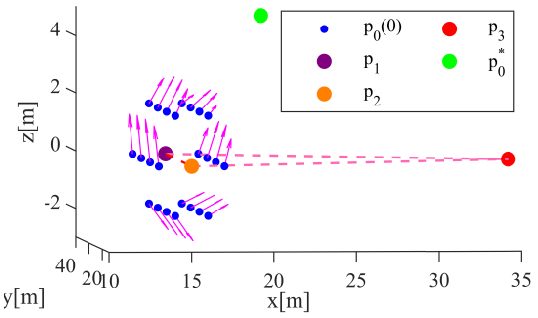

Fig. 3: Velocity direction of vehicle 0 under different initial conditions. In this figure, p_1, p_2, and p_3 denote the positions of the ground stations, p_0^* is the target position, and $p_0(0)$ is the initial position which is set near the line connecting p_1 and p_2. The arrows indicate the direction of the agent's velocity under different initial conditions. The figure illustrates that when the agent is close to the line connecting p_1 and p_2, it moves away from the line and moves toward the target position.

Only two cases are possible, namely $\alpha_{012}(T_1^-)\to 0^+$ or $\alpha_{012}(T_1^-)\to\pi^-$. Since α_{012}^* is bounded away from zero and π. For the case $\alpha_{012}(T_1^-)\to 0^+$, one has $e_1(T_1^-)=\alpha_{012}(T_1^-)-\alpha_{012}^*(T_1^-)<0$. Note that $\sin\alpha_{102}(T_1^-)>0$ and $l_{20}(T_1^-)>0$. According to (11), $\dot e_1(T_1^-)>0$, which implies that $\alpha_{102}(t)$ will increase from $t=T_1^-$ to $t=T_1$ instead of reaching $\alpha_{102}(T_1)=0$. Therefore, $p_0(t)$ will not be colinear with p_1, p_2.

An illustration is shown as Fig. 3. When the agent is close to the line $\overleftrightarrow{p_1p_2}$, it's velocity vector filed points away from the line $\overleftrightarrow{p_1p_2}$, demonstrating that no collinearity and collision will occur. ■

Now, we analyze the bounds of the coefficients in the dynamics (11), (13) and (18). Then, we prove that $\sin\alpha_{021}(t), \sin\alpha_{102}(t), l_{10}(t), l_{20}(t)$ will be upper and lower bounded. Since no collinearity and collision will happen among the aircraft and the ground stations, the dynamics (19) imply that $|e_1(t)|, |e_2(t)|, |e_p(t)|$ will decrease monotonously. Therefore, one has

$$0<\min\{\alpha_{012}(0),\alpha_{012}^*\}\le\alpha_{012}(t)\le\max\{\alpha_{012}(0),\alpha_{012}^*\}<\pi$$

The same case applies for $\alpha_{021}(t)$, i.e.,

$$0<\min\{\alpha_{021}(0),\alpha_{021}^*\}\le\alpha_{021}(t)\le\max\{\alpha_{021}(0),\alpha_{021}^*\}<\pi$$

It follows that

$$0<\pi-\max\{\alpha_{012}(0),\alpha_{012}^*\}-\max\{\alpha_{021}(0),\alpha_{021}^*\}\le\alpha_{102}(t)\le\pi-\min\{\alpha_{012}(0),\alpha_{012}^*\}-\min\{\alpha_{021}(0),\alpha_{021}^*\}<\pi$$

Therefore, the angles $\alpha_{012}(t), \alpha_{021}(t), \alpha_{102}(t)$ are all bounded away from zero and π. Then, we analyze the bounds of $l_{01}(t)$ and $l_{02}(t)$. Using the law of sines, one has

$$0<\frac{l_{12}\sin\alpha_{021}^{\text{lower}}}{\sin\alpha_{102}^{\text{upper}}}\le l_{01}(t)=\frac{l_{12}\sin\alpha_{021}(t)}{\sin\alpha_{102}(t)}\le\frac{l_{12}\sin\alpha_{021}^{\text{upper}}}{\sin\alpha_{102}^{\text{lower}}}$$

where $\alpha_{021}^{\text{lower}}=\{\alpha|\min_{\alpha}\sin\alpha,\alpha\in(\min\{\alpha_{021}(0),\alpha_{021}^*\},\max\{\alpha_{021}(0),\alpha_{021}^*\})\}$, $\alpha_{021}^{\text{upper}}=\{\alpha|\max_{\alpha}\sin\alpha,\alpha\in(\min\{\alpha_{021}(0),\alpha_{021}^*\},\max\{\alpha_{021}(0),\alpha_{021}^*\})\}$ and $\alpha_{102}^{\text{lower}},\alpha_{102}^{\text{upper}}$ can be similarly defined. Similarly, one also has

$$0<\frac{l_{12}\sin\alpha_{012}^{\text{lower}}}{\sin\alpha_{102}^{\text{upper}}}\le l_{02}(t)=\frac{l_{12}\sin\alpha_{012}(t)}{\sin\alpha_{102}(t)}\le\frac{l_{12}\sin\alpha_{012}^{\text{upper}}}{\sin\alpha_{102}^{\text{lower}}}$$

Finally, since $|\alpha_p(t)-\alpha_p^*|$ decrease monotonously, one also has

$$-\pi<\min\{\alpha_p(0),\alpha_p^*\}\le\alpha_p(t)\le\max\{\alpha_p(0),\alpha_p^*\}<\pi$$

Based on the above bounded results, we can now analyze the system convergence.

C. Convergence analysis

Although the system matrix of the overall dynamics (19) is a diagonal matrix, the elements of the diagonal matrix are state-dependent and time-varying, which makes (19) nonlinear. Before giving the convergence result, we first present a lemma.

Lemma 3 ([20]): Let $W(\cdot):\mathbb{R}^+\to\mathbb{R}^{m\times r}$ be regulated, $x\in\mathbb{R}^m$, and $m\in\mathbb{N}^+, r\in\mathbb{N}^+$. Then

$$\dot x(t)=-W(t)W^\top(t)x(t) \tag{20}$$

is globally and exponentially stable if and only if there exist positive scalars T_2,γ_1,γ_2 such that for $\forall t>0$, $\gamma_1 I_{m\times m}\le\int_t^{t+T_2}\left(W(\tau)W^\top(\tau)\right)d\tau\le\gamma_2 I_{m\times m}$. □

Based on (3), we present the main result now.

Theorem 1: Given three static ground stations and the aircraft governed by (5), if $p_0(0)$ is bounded away from $\overleftrightarrow{p_1p_2}$, then the three angle errors globally and exponentially converge to zero, and $p_0(t)$ globally and asymptotically converges to the target position p_0^*.

Proof: First, we rewrite the closed-loop angle error dynamics (19) as $\dot X=-Q(t)Q(t)^\top X$, $X=[e_1,e_2,e_p]^\top$, $Q(t)=\text{diag}\left(\sqrt{\frac{\sin\alpha_{102}}{l_{10}}},\sqrt{\frac{\sin\alpha_{102}}{l_{20}}},\sqrt{\frac{\sin\alpha_{102}}{l_{20}\sin\alpha_{021}}}\right)$ Then, for every $t>0$, $\beta_1 I_3\le\int_t^{t+T}Q(\tau)Q^\top(\tau)\text{d}\tau\le\beta_2 I_3$ where $T>0$,

$$\beta_1=\frac{(\sin\alpha_{102}^{\text{lower}})^2T}{l_{12}\max\{\sin\alpha_{021}^{\text{upper}},\sin\alpha_{012}^{\text{upper}},\sin\alpha_{012}^{\text{upper}}\sin\alpha_{021}^{\text{upper}}\}},$$
$$\beta_2=\frac{(\sin\alpha_{102}^{\text{upper}})^2T}{l_{12}\min\{\sin\alpha_{021}^{\text{lower}},\sin\alpha_{012}^{\text{lower}},\sin\alpha_{012}^{\text{lower}}\sin\alpha_{021}^{\text{lower}}\}}.$$

According to Lemma 3, $e_1(t), e_2(t), e_p(t)$ converge to zero globally and exponentially. According to Lemma 1, one has that $p_0(t)$ asymptotically and globally converges to the target position p_0^*. ■

Remark 4: Indeed, since the desired position and the agent's real-time position are unknown, the agent cannot move directly towards the desired position, for which the agent's moving trajectory may not be optimal. In addition, communication is needed between the agent and the ground stations, in which communication delays are inevitable. However, since the desired position is only equilibrium of the angle constraints, small delay may not affect the overall closed-loop

performance. To mitigate the negative effect of communication delays, the implementation of the algorithm can be based on high advanced communication technology, such as 5G.

Remark 5: By describing the target position through ratio of distances and angles, global stabilization is achieved in [19] where only local bearing and ratio of distance measurements are needed. However, through detection algorithms in computer vision, obtaining accurate ratio-of-distance information in 3D is challenging. The squared area of a neighboring agent in the image plane depends not only on its distance but also its attitude. Variations in agents' relative attitudes can cause significant changes in the projected squared area, which can make the measurements unreliable. Compared with [19], the cost of our solution is the need of communication, and the benefit of our solution is the no need of ratio of distance measurements. Since $\alpha^*_{012}, \alpha^*_{021}, \alpha^*_p$ are scalars instead of vectors, they are independent of the aircraft's inertial frame. The aircraft cannot obtain $\alpha_{012}, \alpha_{021}, \alpha_p$ directly from its local bearing measurements b_{01}, b_{02}, b_{03}. Angles $\alpha_{012}, \alpha_{021}, \alpha_p$ measured by static ground stations need to be communicated from the ground stations to the aircraft. This communication cannot be avoided in this work where global convergence is aimed to achieve.

Remark 6: In Theorem 1, no matter whether $p_0(0)$ is in positive or negative direction w.r.t $\mathbb{P}_{123}$, the vehicle can converge to the right equilibrium eventually. This is not achieved in the previous 3-D angle-based laws [13].

D. Robustness analysis

Consider agent 0's dynamic model as $\dot{p}_0(t) = u_0(t) + d(t)$, where $d(t) \in \mathbb{R}^3$ represents the environmental factors. Under these environmental factors, such as disturbances, communication delays or sensor inaccuracies, the overall closed-loop dynamics $\dot{X} = A(X)X$ in 19 will be changed to

$$\dot{X} = A(X)X + g(t, X) \tag{21}$$

where $g(t, X) \in \mathbb{R}^3$ is the perturbation term. Suppose that $\|g(t, X)\| \leq \gamma \|X\|$. Then, for the perturbed dynamics (21), depending on whether $g(t, X)$ is vanishing (such as communication delays) or non-vanishing (such as disturbance and sensor inaccuracies), one has the following results.

Proposition 1: [21, Lemma 9.1] For (21), if it well-defined for $t \geq 0$ and $g(t, X)$ is vanishing, then $X = 0$ is still an equilibrium of (21). Moreover, if $\gamma < 2\beta_1$ and $l_{10}(t) \neq 0, l_{20}(t) \neq 0, \sin\alpha_{021}(t) \neq 0, \forall t \geq 0$, then the origin $X(t) = 0$ is an exponentially stable equilibrium point of the perturbed system (21).

The proof of the above proposition is straightforward by setting Lyapunov function $V(X) = X^\top X$ and $c_3 = \beta_1$ and $c_4 = 2$ in [21, Lemma 9.1].

Proposition 2: [21, Lemma 9.2] For (21), if it is well-defined for $t \geq 0$ and $g(t, X)$ is non-vanishing, then $X = 0$ is generally not an equilibrium of (21). Moreover, if $\gamma < 4\beta_1\pi\theta$ with some positive constant $\theta < 1$ and $l_{10}(t) \neq 0, l_{20}(t) \neq 0, \sin\alpha_{021}(t) \neq 0, \forall t \geq 0$, then the solution $X(t)$ is uniformly ultimately bounded under the perturbed dynamics (21).

The proof of the above proposition is straightforward by setting $c_3 = \beta_1$, $c_4 = 2$, $c_1 = 1/4$ and $c_2 = 1$ in [21, Lemma 9.1]. Indeed, the above results depend on γ, whose value depends on the specific form of the perturbation term $g(t, X)$, namely the specific form of the disturbing factors. Note that the conclusions in Propositions 1 and 2 hold only when the perturbed dynamics (21) are well-defined for all $t \geq 0$. This requires that the system avoids collinear scenarios and collision among vehicle 0 and stations 1 and 2, which can be described by $l_{10}(t) \neq 0, \quad l_{20}(t) \neq 0, \quad \sin\alpha_{021}(t) \neq 0, \quad \forall t \geq 0$. Indeed, this is not guaranteed in the dynamics (21), especially when $g(t, X)$ does not vanish.

IV. Extension to angle-based control for quadrotor model

As an extension, we discuss the application of angle-based control to quadrotor model where our aim is to achieve at least local convergence. The position and attitude dynamics of the quadrotor UAV can be described as [22]

$$m_0\ddot{p}_0 + m_0 g z_G = u_0, \tag{22}$$

$$J_0(\Theta_0)\ddot{\Theta}_0 + C_0(\Theta_0, \dot{\Theta}_0)\dot{\Theta}_0 = \tau_0 \tag{23}$$

where $m_0 \in \mathbb{R}^+$ is the UAV's mass, $g \in \mathbb{R}$ is the gravitational acceleration constant, $z_G = [0, 0, 1]^{\mathrm{T}}$, $u_0 \in \mathbb{R}^{3\times1}$ is the applied translational control force, $\tau_0 \in \mathbb{R}^{3\times1}$ is the applied rotational control torque, $J_0(\Theta_0) \in \mathbb{R}^{3\times3}$ is rotational inertia matrix, and $\Theta_0 \in \mathbb{R}^3$ represents the attitude angles of the UAV. Here, we only investigate the control design for the position dynamics (22). Since the quadrotor dynamics is under-actuated, according to [22], once the control force u_0 is designed and the desired yaw angle is specified, the desired yaw and pitch angles are directly determined, after which the rotating speed of the four rotors in the quadrotor can also be determined. Now, we design the position control law as

$$\begin{aligned} u_0 = {} & m_0 g z_G - k_v\dot{p}_0 - m_0(\alpha_p(t) - \alpha^*_p)b_{01}(t) \times b_{02}(t) \\ & + m_0(\alpha_{012}(t) - \alpha^*_{012})b_{02}(t) + m_0(\alpha_{021}(t) - \alpha^*_{021})b_{01}(t) \end{aligned} \tag{24}$$

Then, we have the following results.

Theorem 2: Given three static ground stations and the aircraft governed by (22), the three angle errors exponentially converge to zero, and $p_0(t)$ asymptotically converges to the target position p^*_0.

Proof: We also analyze the angle error dynamics. In the case of single-integrator dynamics, the state space consists of three angle errors. However, for quadrotor model with double-integrator dynamics, the state space consists of three angle errors and the vehicle's velocity. Their dynamics can be described as

$$\dot{e}_1 = -\frac{b_{12}^\top P_{b_{10}}\dot{p}_0}{l_{10}\sin\alpha_{012}}, \quad \dot{e}_2 = -\frac{b_{21}^\top P_{b_{20}}\dot{p}_0}{l_{20}\sin\alpha_{021}}$$

$$\dot{e}_p = -\frac{n_{123}^\top P_{n_{012}}(\frac{P_{b_{20}}\dot{p}_0}{l_{20}} \times b_{21})}{\|b_{20} \times b_{21}\|\sin\alpha_p} = -\frac{n_{123}^\top P_{n_{012}} b_{21}^\times P_{b_{20}}\dot{p}_0}{\|b_{20} \times b_{21}\| l_{20}\sin\alpha_p}$$

$$\ddot{p}_0 = -\frac{k_v}{m_0}\dot{p}_0 + e_1 b_{02} + e_2 b_{01} - e_p b_{01} \times b_{02} \tag{25}$$

where $b_{21}^{\times} = \begin{bmatrix} 0 & -b_{21}(3) & b_{21}(2) \\ b_{21}(3) & 0 & -b_{21}(1) \\ -b_{21}(2) & b_{21}(1) & 0 \end{bmatrix}$. Then, the compact form of the overall dynamics can be written by

$$\dot{Y} = A(Y)Y = \begin{bmatrix} 0 & 0 & 0 & -\frac{b_{12}^{\top} P_{b_{10}}}{l_{10} \sin \alpha_{012}} \\ 0 & 0 & 0 & -\frac{b_{21}^{\top} P_{b_{20}}}{l_{20} \sin \alpha_{021}} \\ 0 & 0 & 0 & -\frac{n_{123}^{\top} P_{n_{012}} b_{21}^{\times} P_{b_{20}}}{\|b_{20} \times b_{21}\| l_{20} \sin \alpha_p} \\ b_{02} & b_{01} & -b_{01} \times b_{02} & -k_v/m_0 I_3 \end{bmatrix} Y \tag{26}$$

where $Y = \begin{bmatrix} e_1 & e_2 & e_p & \dot{p}_0^{\top} \end{bmatrix}^{\top}$. According to [12], conducting linearization for the dynamics (26) around the desired equilibrium $Y = 0$ yields

$$\dot{Y} = A^* Y = \begin{bmatrix} 0 & 0 & 0 & -\frac{b_{12}^{*\top} P_{b_{10}^*}}{l_{10}^* \sin \alpha_{012}^*} \\ 0 & 0 & 0 & -\frac{b_{21}^{*\top} P_{b_{20}^*}}{l_{20}^* \sin \alpha_{021}^*} \\ 0 & 0 & 0 & -\frac{n_{123}^{*\top} P_{n_{012}^*} b_{21}^{*\times} P_{b_{20}^*}}{\|b_{20}^* \times b_{21}^*\| l_{20}^* \sin \alpha_p^*} \\ b_{02}^* & b_{01}^* & -b_{01}^* \times b_{02}^* & -k_v I_3/m_0 \end{bmatrix} Y$$
$$= \begin{bmatrix} 0_{3\times 3} & C^* \\ D^* & -k_v I_3/m_0 \end{bmatrix} Y \tag{27}$$

where b_{12}^*, α_{012}^*, etc represent the desired bearing vector, angle, etc, respectively at the desired equilibrium $Y = 0$, $C^* \in \mathbb{R}^{3\times 3}$, and $D^* \in \mathbb{R}^{3\times 3}$. To evaluate the stability of the linear dynamics (27), we analyze the eigenvalues of A^*, i.e.,

$$\begin{aligned} |\lambda I_6 - A^*| &= \begin{vmatrix} \lambda I_3 & -C^* \\ -D^* & (\lambda + k_v/m_0) I_3 \end{vmatrix} \\ &= \det[\lambda(\lambda + \frac{k_v}{m_0}) I_3 - C^* D^*] \\ &= \left[\lambda(\lambda + \frac{k_v}{m_4}) + \frac{\sin \alpha_{102}^*}{l_{10}^*}\right] \left[(\lambda(\lambda + \frac{k_v}{m_4}) + \frac{\sin \alpha_{102}^*}{l_{20}^*}\right] \\ &\quad \times \left[\lambda(\lambda + \frac{k_v}{m_4}) + \frac{\sin \alpha_{102}^*}{l_{20}^* (\sin \alpha_{021}^*)}\right] \end{aligned} \tag{28}$$

where $\cos \theta^* = n_{123}^{*\top} b_{20}^* > 0$, and we have used the fact that $C^* D^* = \text{diag}[-\frac{\sin \alpha_{102}^*}{l_{10}^*}, -\frac{\sin \alpha_{102}^*}{l_{20}^*}, -\frac{\sin \alpha_{102}^*}{l_{20}^* (\sin \alpha_{021}^*)}]$. It becomes straightforward from the characteristic polynomial (28) that all the six eigenvalues of A^* have negative real parts, which implies the asymptotic stability of (27), i.e., $p_0(t)$ asymptotically converges to the target position p_0^*. ■

Remark 7: Since the system matrix in the closed-loop dynamics (26) does not have a diagonal form and linearization analysis is conducted, only local convergence is obtained for the quadrotor model in this section.

V. Simulation Results

In this section, we conduct simulations for the proposed control laws. The used simulation software is Matlab and Simulink.

A. Single-integrator model

To verify Theorem 1, we consider that the vehicle's target position is $p_0^* = [15; 25; 10]$ and the ground stations' positions are $p_1 = [0; 0; 0]$, $p_2 = [17; 10; 0]$ and $p_3 = [0; 20; 0]$.

In the first case, we consider $p_0(0) = [50; 37; 29]$ lies in the positive direction w.r.t $\mathbb{P}_{123}$. The results shown in Fig. 4 demonstrate Theorem 1. In the second case, we consider $p_0(0) = [50; 37; -29]$ lies in the negative direction w.r.t $\mathbb{P}_{123}$. The results are shown in Fig. 5 demonstrate Remark 6. In the third case, we consider that the vehicle's local coordinate frame $\sum_i$ has 5° rotation along x-axis, 6° rotation along y-axis, 7° rotation along z-axis with respect to the global coordinate frame $\sum_g$. The results shown in Fig. 6 demonstrate that the vehicle's local coordinate frame has no impact on the evolution of the system convergence.

To simulate disturbances, we incorporate Gaussian white noise into the single-integrator model (4). The simulation results are shown in Fig. 7a, which reveals that the proposed control law possesses a certain level of disturbance rejection capability. We also simulate the case where the communicated

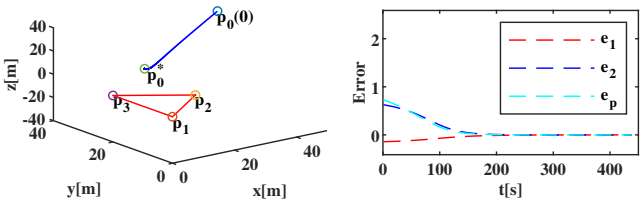

(a) Moving trajectory (b) Evolution of angle errors

Fig. 4: $p_0(0)$ is in the positive direction w.r.t. $\mathbb{P}_{ijk}$

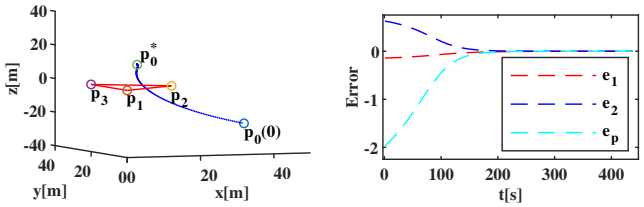

(a) Moving trajectory (b) Evolution of angle errors

Fig. 5: $p_0(0)$ is in the negative direction w.r.t. $\mathbb{P}_{123}$

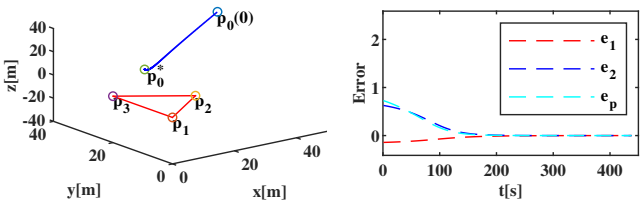

(a) Moving trajectory (b) Evolution of angle errors

Fig. 6: Vehicle 0 has a local coordinate frame

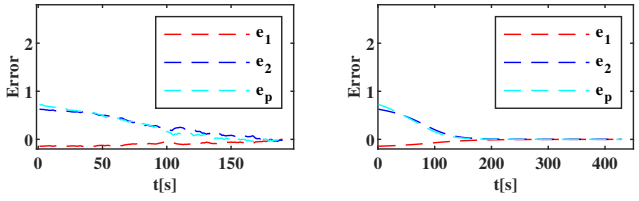

(a) Evolution of angle errors under disturbances (b) Evolution of angle errors under communication delay

Fig. 7: Robustness against disturbances and communication delay

angles $\alpha_{012}, \alpha_{021}, \alpha_p$ have delay of 10 simulation time steps. The result in Fig. 7b demonstrates that the equilibrium is still the origin, which validates Proposition 1.

B. Quadrotor model

To verify Theorem 2, we use the same parameters as those in Fig. 4. The simulation results are given in Fig. 8, which demonstrate the asymptotic stability given in Theorem 2. Monte Carlo simulations are also conducted in Fig. 9, in which convergence consistency w.r.t the agent's initial positions are found.

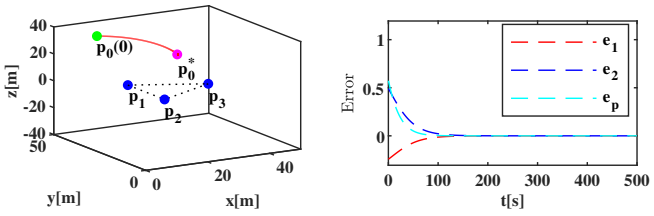

(a) Moving trajectory (b) Evolution of angle errors

Fig. 8: The simulation results of the quadrotor model.

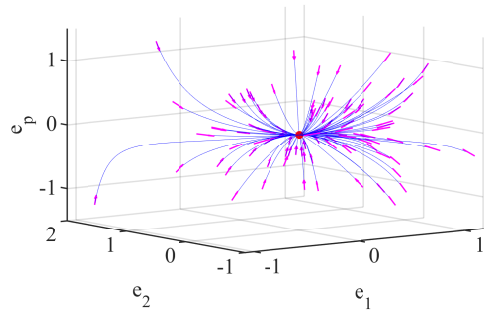

Fig. 9: Monte Carlo simulations for the closed-loop dynamics of the quadrotor model

VI. Conclusion

In this paper, we have developed a novel 3-D angle-based control law that enables an aircraft to autonomously reach a target location by relying solely on local direction measurements with respect to three ground stations. Unlike conventional control methods, the proposed approach guarantees global convergence to the target location while remaining independent of the aircraft's coordinate frame orientation. These properties make the control law particularly suitable for scenarios where relative position measurements are unreliable or inaccessible. The practical significance of this work lies in its potential applications to autonomous aerial navigation, such as UAV missions in GPS-denied environments or areas with limited sensor capabilities. Future research could explore extending the approach to dynamic ground stations, incorporating more complex aircraft dynamics. In addition, the measurement and control processes could be modeled in discrete time to better reflect real-world implementation on digital processors.

References

[1] H. Shakhatreh, A. H. Sawalmeh, A. Al-Fuqaha, Z. Dou, E. Almaita, I. Khalil, N. S. Othman, A. Khreishah, and M. Guizani, "Unmanned aerial vehicles (UAVs): A survey on civil applications and key research challenges," *IEEE Access*, vol. 7, pp. 48 572–48 634, 2019.

[2] A. Hafeez, M. A. Husain, S. Singh, A. Chauhan, M. T. Khan, N. Kumar, A. Chauhan, and S. Soni, "Implementation of drone technology for farm monitoring & pesticide spraying: A review," *Information processing in Agriculture*, 2022.

[3] F. Syed, S. K. Gupta, S. Hamood Alsamhi, M. Rashid, and X. Liu, "A survey on recent optimal techniques for securing unmanned aerial vehicles applications," *Transactions on Emerging Telecommunications Technologies*, vol. 32, no. 7, p. e4133, 2021.

[4] Z. M. Kassas, P. Closas, and J. Gross, "Navigation systems panel report navigation systems for autonomous and semi-autonomous vehicles: Current trends and future challenges," *IEEE Aerospace and Electronic Systems Magazine*, vol. 34, no. 5, 2019.

[5] H. Teimoori and A. V. Savkin, "Equiangular navigation and guidance of a wheeled mobile robot based on range-only measurements," *Robotics and Autonomous Systems*, vol. 58, no. 2, pp. 203–215, 2010.

[6] T.-M. Nguyen, Z. Qiu, M. Cao, T. H. Nguyen, and L. Xie, "Single landmark distance-based navigation," *IEEE Transactions on Control Systems Technology*, vol. 28, no. 5, pp. 2021–2028, 2019.

[7] S. U. Kamat and K. Rasane, "A survey on autonomous navigation techniques," in *2018 Second International Conference on Advances in Electronics, Computers and Communications (ICAECC)*, 2018, pp. 1–6.

[8] T. D. Nguyen, "Evaluation of the accuracy of the ship location determined by GPS global positioning system on a given sea area," in *Journal of Physics: Conference Series*, vol. 1515, no. 4. IOP Publishing, 2020, p. 042010.

[9] Z. Meng, B. D. Anderson, and S. Hirche, "Formation control with mismatched compasses," *Automatica*, vol. 69, pp. 232–241, 2016.

[10] H. G. de Marina, "Maneuvering and robustness issues in undirected displacement-consensus-based formation control," *IEEE Transactions on Automatic Control*, vol. 66, no. 7, pp. 3370–3377, 2020.

[11] M. H. Trinh, G.-H. Ko, V. H. Pham, K.-K. Oh, and H.-S. Ahn, "Guidance using bearing-only measurements with three beacons in the plane," *Control Engineering Practice*, vol. 51, pp. 81–91, 2016.

[12] L. Chen, M. Cao, and C. Li, "Angle rigidity and its usage to stabilize multiagent formations in 2-D," *IEEE Transactions on Automatic Control*, vol. 66, no. 8, pp. 3667–3681, 2020.

[13] L. Chen and M. Cao, "Angle rigidity for multi-agent formations in 3-D," *IEEE Transactions on Automatic Control*, vol. 68, no. 10, pp. 6130–6145, 2023.

[14] T. Nguyen, Z. Qiu, M. Cao, T. Nguyen, and L. Xie, "An integrated localization-navigation scheme for distance-based docking of UAVs," in *2018 IEEE/RSJ International Conference on Intelligent Robots and Systems (IROS)*. IEEE, 2018, pp. 5245–5250.

[15] M. Basiri, A. N. Bishop, and P. Jensfelt, "Distributed control of triangular formations with angle-only constraints," *Systems and Control Letters*, vol. 59, no. 2, pp. 147–154, 2010.

[16] S. Minaeian, J. Liu, and Y.-J. Son, "Vision-based target detection and localization via a team of cooperative uav and ugvs," *IEEE Transactions on Systems, Man, and Cybernetics: Systems*, vol. 46, no. 7, pp. 1005–1016, 2015.

[17] P. Sambu and M. Won, "An experimental study on direction finding of bluetooth 5.1: Indoor vs outdoor," in *2022 IEEE Wireless Communications and Networking Conference (WCNC)*. IEEE, 2022, pp. 1934–1939.

[18] M. S. Guzel and R. Bicker, "Vision based obstacle avoidance techniques," *Recent advances in mobile robotics*, pp. 83–108, 2011.

[19] O. Mirzaeedodangeh, F. Mehdifar, and D. V. Dimarogonas, "3D directed formation control with global shape convergence using bispherical coordinates," *arXiv preprint arXiv:2403.13609*, 2024.

[20] B. Anderson, "Exponential stability of linear equations arising in adaptive identification," *IEEE Transactions on Automatic Control*, vol. 22, no. 1, pp. 83–88, 1977.

[21] H. K. Khalil, *Nonlinear systems*. Prentice hall Upper Saddle River, NJ, 2002, vol. 3.

[22] B. Xiao and S. Yin, "A new disturbance attenuation control scheme for quadrotor unmanned aerial vehicles," *IEEE Transactions on Industrial Informatics*, vol. 13, no. 6, pp. 2922–2932, 2017.